New Insights into Aerospace Engineering

Ted Dunham

Volume I

New Insights into Aerospace Engineering

Volume I

Edited by **Ted Dunham**

LANRYE
INTERNATIONAL

New Jersey

Published by Clanrye International,
55 Van Reypen Street,
Jersey City, NJ 07306, USA
www.clanryeinternational.com

New Insights into Aerospace Engineering: Volume I
Edited by Ted Dunham

International Standard Book Number: 978-1-63240-380-3 (Hardback)

Printed in China.

Preface

If we turn the pages of history all the world over, the first aviation pioneers can be traced to the late 19th to early 20th centuries. One of the most prominent names in the history of aeronautics is of Sir George Cayley, who contributed significantly to this field from the last decade of the 18th to mid-19th century. The first definition of aerospace engineering appeared in the month of February in the year 1958.

There are two main branches of this field of engineering, commonly known as aeronautical engineering and astronautical engineering. There is a vast difference between these two sub branches, as aeronautical engineering deals with aircrafts that are operational in Earth's atmosphere, and astronautical engineering studies about the space craft which are basically operational outside the Earth's atmosphere. Aerospace engineering also studies about the aerodynamic characteristics of a spacecraft.

Given the demanding conditions that flight vehicles are often subjected to, both in the earth's atmosphere and outside it, aerospace engineering has seen some rapid growth in the past few decades. Evolving designs, improved safety features, technical and technological improvements, and comfort, all form part of this branch of engineering. The development and manufacturing of a modern flight vehicle is an extremely complex process. Aerospace engineers design, test, and supervise the manufacture of aircraft, spacecraft, and missiles. Aerospace engineers develop new technologies for use in aviation, defense systems, and space. This branch has crucial uses in both civil and military contexts. This book takes a look at both.

I would like to thank all the contributing authors for their time and efforts. I would also like to thank my family and friends for their constant support.

Editor

Contents

Recent Experimental Efforts on High-Pressure Supercritical Injection for Liquid Rockets and Their Implications

Bruce Chehroudi

Advanced Technology Consultants, Laguna Niguel, CA 92677, USA

Correspondence should be addressed to Bruce Chehroudi, chehroudib@aol.com

Academic Editor: David Greatrix

Pressure and temperature of the liquid rocket thrust chambers into which propellants are injected have been in an ascending trajectory to gain higher specific impulse. It is quite possible then that the thermodynamic condition into which liquid propellants are injected reaches or surpasses the critical point of one or more of the injected fluids. For example, in cryogenic hydrogen/oxygen liquid rocket engines, such as Space Shuttle Main Engine (SSME) or Vulcain (Ariane 5), the injected liquid oxygen finds itself in a supercritical condition. Very little detailed information was available on the behavior of liquid jets under such a harsh environment nearly two decades ago. The author had the opportunity to be intimately involved in the evolutionary understanding of injection processes at the Air Force Research Laboratory (AFRL), spanning sub- to supercritical conditions during this period. The information included here attempts to present a coherent summary of experimental achievements pertinent to liquid rockets, focusing only on the injection of nonreacting cryogenic liquids into a high-pressure environment surpassing the critical point of at least one of the propellants. Moreover, some implications of the results acquired under such an environment are offered in the context of the liquid rocket combustion instability problem.

1. Introduction

In designs of chemical rocket engines, liquid fuel and oxidizer are often injected as round jets into a hot and elevated-pressure environment of the thrust chamber. The coaxial and impinging jets injectors are two of the well-established designs in liquid rocket engines (LREs). On the other hand, higher specific impulse is a major motivation for operating rocket thrust chambers at progressively higher pressures. Conditions therefore exist in which the injected liquid finds itself near or even above the thermodynamic critical point. Examples are Space Shuttle Main Engine and Vulcain (Ariane 5) with liquid H_2/liquid O_2.

In such cases, major changes occur in some important and key properties of a substance as it approaches the thermodynamic critical point. For example, under thermodynamic equilibrium, the distinction between the liquid and gas phases disappears at and above the critical point and hence it is referred to as a "fluid." Also, large changes in density occur near the critical point. The constant-pressure specific heat becomes very large and surface tension vanishes at and beyond the critical point. As the ambient pressure into which a liquid jet is injected increases, the importance of the solubility of ambient gases into the injected liquid phase increases and one should consider multicomponent phase equilibrium information. For mixtures, determination of the critical conditions, called the "critical mixing temperature or pressure", is a complex process; see Bruno and Ely [1] and Lazar and Faeth [2]. For example, when a pure liquid hydrocarbon fuel drop is introduced into a nitrogen gas, a thin layer on its surface is a mixture of dissolved nitrogen and the fuel which spreads spatially in time; see Umemura [3].

Understanding the behavior of jets under supercritical conditions therefore is critical to design and modeling of the liquid rockets, in particular, cryogenic liquid rockets. For this reason, systematic research programs, both experimental and computations, have been initiated in the past 20 years to understand behaviors of jets under transcritical and supercritical conditions both with and without externally forced (acoustic) excitations. The reason the external excitation is considered stems from the combined experimental/theoretical work suggesting that interaction between

acoustic resonance modes of the chamber and the jets could play an important role in combustion instability. The basic premise here is that when an important dynamic feature, such as the injected jet's dark-core or breakup zone, of an injector design becomes sufficiently sensitive to thermofluid parameters of its environment, it is highly likely that this could strengthen the feedback link thought to be critical in the amplification process and hence push the system into an unstable operating regime.

The purpose of this paper is to present an overview of important experimental achievements, characterizing and understanding nonreacting steady liquid jets injected into supercritical conditions, and offer some implications of these results and potential linkages to production engines. It is not the intention of this work to provide a comprehensive review of the subject, rather to present important findings reported in recent decades.

The coverage of the injectors' experimental data in this paper is divided into three parts: single liquid jets, coaxial jets, and impinging jets. However, the treatment for the impinging jets is comparatively shorter due to limited data available extending to supercritical conditions. Two sections are considered for each part. One focuses on jets injected into an environment devoid of any externally imposed acoustic excitations and the other considers the impact of such excitations on jet characteristics. Most cases reviewed here pertain to cryogenic liquid jets with the environment, into which the jets are injected, existing at thermodynamic supercritical temperatures. This is similar to those experienced in cryogenic liquid rocket engines.

2. Single Jet without External Excitation

In this section, relevant experimental work conducted on a single steady round jet injected into an environment lacking any externally imposed acoustic disturbances is considered. The purpose here is to examine the behavior of such jets under high pressures, specifically supercritical conditions. In the selection of candidate cases, the test matrix is chosen to cover supercritical conditions. However, it is preferred that the matrix spans a broader range encompassing both sub- and supercritical conditions because it generally provides a more comprehensive picture of differences and similarities between the two conditions.

Historically, research on supercritical injection of relevance to liquid rockets started with a published work of Newman and Brzustowski [4]. They used a steady CO_2 jet injected into a chamber of pure N_2 and also into mixtures of CO_2 + N_2 at both sub- and supercritical pressures and temperatures. Obviously, if the chamber is at a supercritical pressure, the injected jet pressure is higher and must also be at a supercritical pressure. They showed that when the chamber pressure approached just above the critical pressure of the CO_2, injection of CO_2 into mixtures of CO_2 + N_2 (varying initial CO_2 concentration to change mixture density) widened the visual appearance of the jet. This was explained to be due to changes in chamber-to-injectant density ratio. At a higher chamber supercritical pressure, injection of CO_2 into a pure nitrogen gas, but varying temperature (from sub- to supercritical), caused shortening of both the jet visible length and width with chamber temperature.

Newman and Brzustowski [4] also investigated and explained effects of increased chamber temperature on jet appearance. They found that such effects were due to progressive reduction in ambient gas density, hence lowering surface tension to zero at critical temperature, and to increase in liquid CO_2 evaporation. In other experiments, CO_2 was injected into a mixture of CO_2 + N_2 with fixed but large initial CO_2 mass fraction in order to reduce jet evaporation. The chamber temperature was fixed at a supercritical value, but its pressure was varied from sub- to supercritical pressures. They hypothesized and conjectured that at supercritical chamber temperatures and pressures the jet may be considered as a variable-density single-phase turbulent submerged gas jet. Finally, assuming self-preserving flow, negligible gravity, zero latent heat of vaporization, ideal gas behavior, and thermal equilibrium between gas and drops, they develop a model for predicting the profile of the outer extent of a supercritical steady jet and its centerline mean axial velocity. Comparison of this model with experiment was very poor near the injector exit area where most important and complex processes take place. Hence, the proposed hypothesis was not backed by this effort and the matter remained unresolved.

After the aforementioned initial study, two organizations (DLR in Germany and AFRL in USA) dominated the field by pursuing systematic research programs to understand jet breakup and dynamics under high chamber pressures at, and specifically exceeding, the critical condition of the injectant. The majority of the experimental works presented here is thus coming from these two organizations plus other satellite universities they collaborated and/or supported. Each organization has constructed a unique facility from which most of the results for nonreacting jets were acquired and presented here. For more details on their facility designs readers are referred to their publications, many of which are listed in the references.

Researchers at DLR began working with the most simplest and fundamental of all cases, that is, the injection of a single nonreacting round jet into a quiescent environment. At AFRL, although initially droplet studies were planned and conducted, a transition to jets at high Reynolds numbers of practical interest was initiated by the author of this paper and his team members; for example, see Chehroudi et al. [5]. The injection of jets were studied at various chamber pressures ranging from subcritical to supercritical (mostly at supercritical temperatures), which included chamber pressures representative of those experienced in typical cryogenic liquid rocket engine (LRE). For safety reasons, and for the H_2/LOX liquid rockets, it was preferred to simulate liquid oxygen with liquid nitrogen. Early studies have shown that at a nonreacting condition the injection behaviors of these two fluids were similar. To avoid complications introduced by mixture effects, however, many of these studies involved injection of cryogenic liquid nitrogen (LN_2) into room temperature gaseous nitrogen (GN_2). Critical pressure and temperature of nitrogen are 3.39 MPa and 126.2 K,

respectively. Injections into other ambient gases were also investigated.

The objective of this section of the paper is to present key findings and discuss representative results. In some cases, key conclusions confirmed independently by both organizations (DLR and AFRL) are highlighted when appropriate and if they add to the reader's understanding. Before delving into details of the results, it worth indicating that Mayer et al. [6] were the first to take active steps towards a large-scale facility investigating both single and coaxial cryogenic jets under cold and fired conditions. They used LN_2 jets at 105 K injected into a GN_2 environment at 300 K, but at varying ambient pressures ranging from sub- to supercritical conditions. They reported drastic changes in the jet structure near and above the critical pressure. The jet behaved similar to the classical atomization of liquid fuels, with ligaments and drops, below the critical pressure. Mayer et al. [6] attributed this behavior to a continual decline of surface tension until it vanished at and beyond the critical point.

2.1. Visualization of the Jet Interface. Figure 1 presents results published in a work led by Chehroudi which shows representative images of cryogenic LN_2 jets injected into gaseous nitrogen at 300 K (supercritical in temperature); see Chehroudi et al. [5]. The initial temperature of the jets was measured in a separate experiment and under identical flow conditions with a very small thermocouple. Depending on the flow condition, the measured initial injection temperature varied from 99 K to 110 K, that is, injected at a subcritical value. Pressures in Figure 1 are reported as reduced pressures (P_r), defined to be the chamber pressure divided by the critical pressure of the injected nitrogen. In frames 1 to 4 (of Figure 1), where the chamber pressure is subcritical, the jets have a classical liquid spray appearance. Figure 2 shows magnified images of the three injection cases under sub-, near-, and super-critical chamber pressures. This software magnification is performed to more clearly show the shear layer structure near the injector exit area. As shown in Figure 1, and consistent with the classical liquid jet breakup regimes described by Reitz and Bracco [7], surface instabilities grow downstream from the injector, and very fine ligaments and drops are ejected from the jet (see also the left image in Figure 2). This behavior corresponds to the second wind-induced liquid jet break-up regime described by Reitz and Bracco [7].

Major structural and interfacial changes occur at about $P_r = 1.03$ as shown in frame 5 of Figure 1. Above this chamber pressure, drops are no longer detected, and as characterized by Chehroudi et al. [5], regular "finger-like" entities are observed at the interface. Rather than breaking up into droplets, the interface appears to dissolve at different distances from the dense and dark core. These structures are illustrated at $P_r = 1.22$ in the middle frame of Figure 2. Such a change in morphology of the mixing layer is evidently due to combined effects of the reduction in the surface tension, as the critical pressure is exceeded, and disappearance of the enthalpy of vaporization because of this transition to supercritical pressures.

As the chamber pressure is further increased, the length and thickness of the dense (and dark) core decrease, and the jet begins to appear similar to a turbulent gaseous jet injected into a gaseous environment. This is illustrated in frames 7 and higher in Figure 1. Any further droplet production, and consequently any additional classical liquid atomization, is completely suppressed. These observations were confirmed by Mayer et al. [6, 8], Chehroudi et al. [5], and Roy and Segal [9]. As mentioned earlier, similar results were also found when injecting liquid oxygen instead of the liquid nitrogen.

It is important to indicate that because of the very large density variations between the jet core and the chamber, Chehroudi et al. [5] investigated whether the evolution of the jet within the region of their measurement was affected by the buoyancy forces. Therefore, they calculated the Froude number values under each test condition. As an example, Chehroudi et al. [5, 10] showed that the Froude number ranged from 42,000 to 110,000. To make sense of these values, they looked at the Chen and Rodi [11] results. Chen and Rodi [11] suggested that the flow is momentum dominated when a defined length scale x_b is less than 0.53, while Papanicolaou and List [12] suggested $x_b < 1$. The length scale is given by $x_b = \mathrm{Fr}^{-1/2}(\rho/\rho_\infty)^{-1/4}(x/d)$, where x is the axial distance, d is the initial jet diameter, and ρ and ρ_∞ are the jet and ambient densities, respectively. The Froude number is defined as $\mathrm{Fr} \equiv \rho U^2/gd|\rho_\infty - \rho|$ where U is the velocity difference and g is the gravitational acceleration. Considering a more conservative estimate by Chen and Rodi [11], the jet used by Chehroudi et al. [5, 10] is momentum dominated for distances less than 30 to 40 mm from the injector exit plane. Pictures presented in Figures 1 and 2 cover up to about 5.5 mm (axial distance/diameter ratio of 21.6) from the injector, and hence buoyancy effects can be ignored in favor of inertial forces.

2.2. Length Scale Investigation. Injection of a single LN_2 jet into gaseous N_2 (at 298 K) has been investigated by Branam and Mayer [13] at ambient pressures of 4 MPa and 6 MPa, corresponding to reduced pressures of 1.17 and 1.76, respectively. The initial injection temperature of the nitrogen was near the critical point. They provided a measure of the length scales by analyzing shadowgraph images and called it as the "visible length scale." More details on their image analysis can be found in Branam and Mayer [13].

Figure 3 shows a typical result of the geometrically averaged length scale (average of radial and axial length scales) measured at the x/D of 10 as a function of the radial position. Results from the k-ε computational method are also shown. This suggests that the measured visible length scale is comparable in magnitude to the Taylor length scale determined by the computational method.

The ratio of the axial to the radial length scales indicates whether the visible structures are spherical or more ellipsoidal in shape. Both length scales are shown in Figure 4 for an injection temperature of 123 K, that is, injection of N_2 at a high density. In the near-injector region, the axial length scales are much larger than the radial ones. Further downstream, however, the visible structures become more

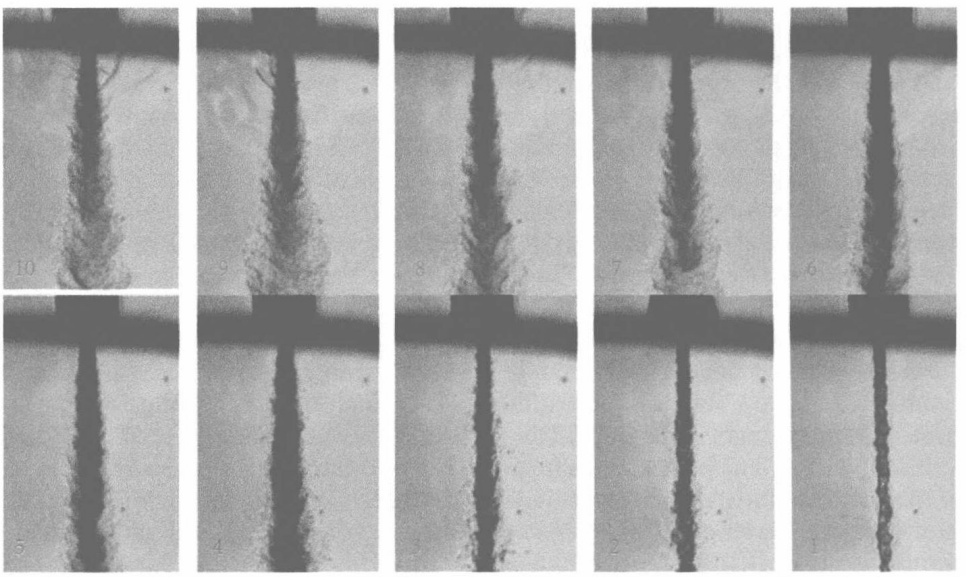

FIGURE 1: Back-illuminated images of a single nitrogen jet injected into nitrogen at a fixed supercritical temperature of 300 K but varying sub- to supercritical pressures (For N_2: $P_{critical}$ = 3.39 MPa; T_c = 126.2 K). From lower right to upper left: $P_{ch}/P_{critical}$ (frame no.) = 0.23 (1), 0.43 (2), 0.62 (3), 0.83 (4), 1.03 (5), 1.22 (6), 1.62 (7), 2.44 (8), 2.74 (9). Reynolds' number (Re) was from 25,000 to 75,000. Injection' velocity: 10–15 m/s. Froude' number: 40,000 to 110,000. Injectant temperature: 99 to 120 K. Chehroudi et al. [5].

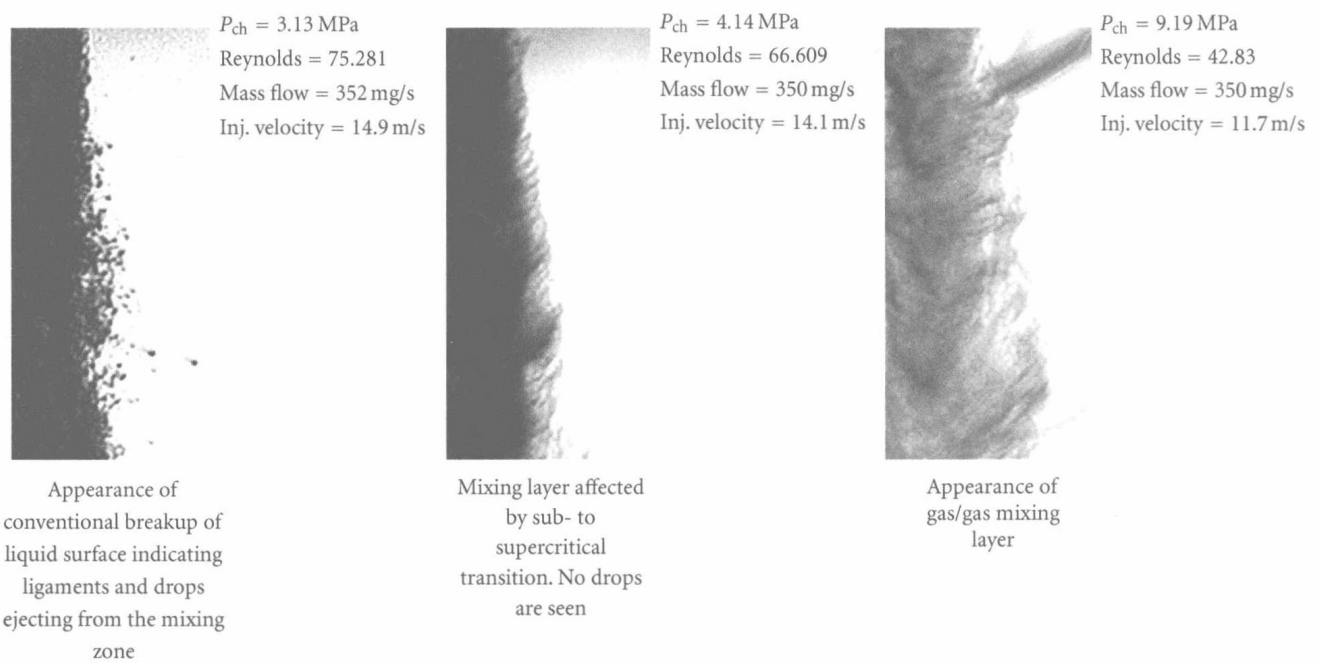

FIGURE 2: Software magnified images of the jets in Figure 1 at their outer boundaries showing transition to the gas-jet-like appearance starting at just below the critical pressure of the injectant. Images are at fixed supercritical chamber temperature of 300 K. Chehroudi et al. [5].

circular in shape. At a higher injection temperature (132 K), the asymmetry between the radial and axial length scales is not as pronounced as that seen under the lower temperature condition (123 K).

2.3. Jet Spreading Angle or Growth Rate. Measurements and estimations of the growth rate of a jet have been a subject of intense research for years because it provides a primary measure of mixing and development of the jet itself. Chehroudi's group was the first to extract quantitative measurements of this physical parameter using the images taken from a cryogenic N_2 jet injected into GN_2 under both subcritical and supercritical pressures; see Chehroudi et al. [5]. These measurements led to important conclusions regarding the character of the growth rate and the behavior of the jet near the injector and under such conditions, specifically at supercritical chamber pressures.

The spreading angle or growth rate was measured from a field of view within 5.5 mm of the injector exit plane (distance-to-diameter ratio of up to 21.6) and was inertially

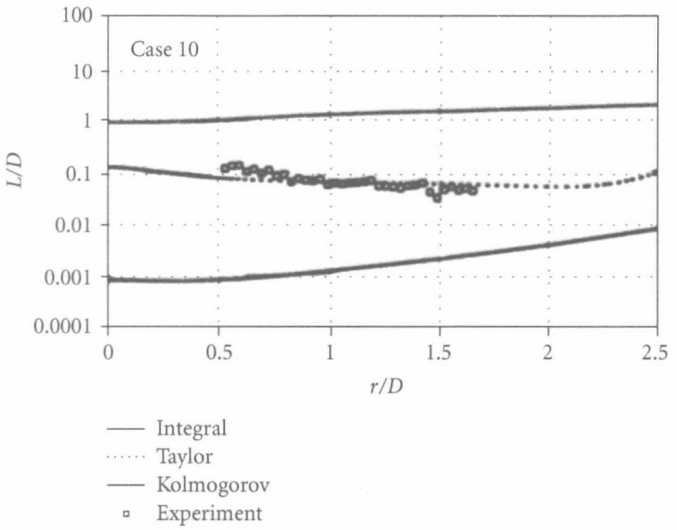

FIGURE 3: Comparison between calculated and experimental length scales for a single jet of LN_2 injected into GN_2 at $x/d = 10$, chamber pressure of 6 MPa, 1.9 m/s, injected temperature of $T = 132$ K. Branam and Mayer [13].

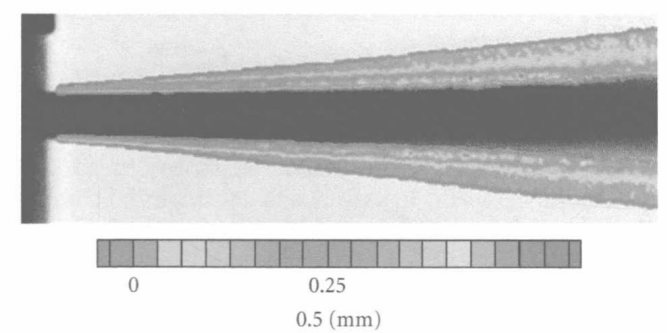

(a) Radial length scale

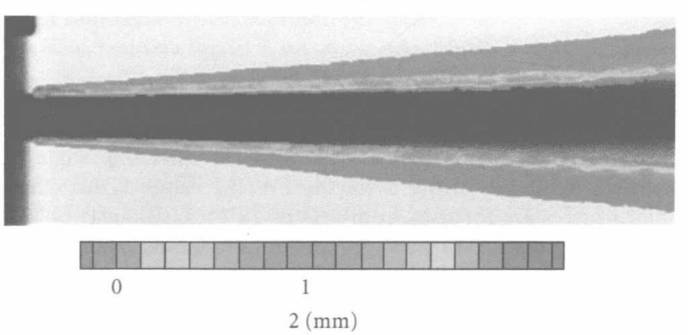

(b) Axial length scale

FIGURE 4: Experimental length scales for LN_2 into GN_2, chamber pressure of 4 MPa, LN_2 injected temperature of 123 K. Branam and Mayer [13].

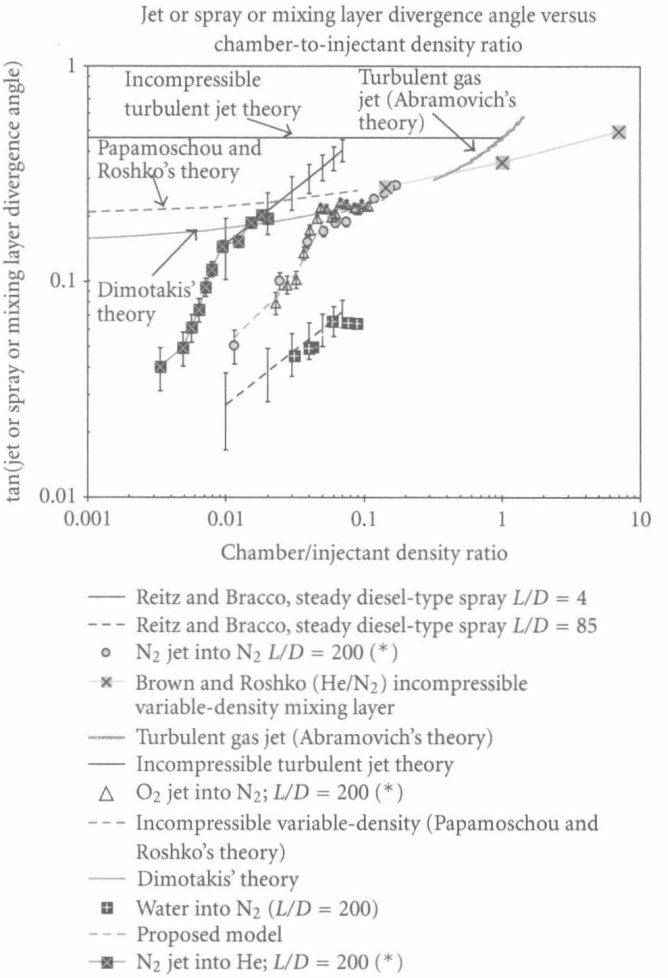

FIGURE 5: Spreading or growth rate of single jets as a tangent of the visual spreading angle versus the chamber-to-injectant density ratio. Data taken by Chehroudi are indicated by an asterisk (*) in the legend. Chehroudi et al. [5].

dominated as discussed earlier. Chehroudi et al. [5] indicated that their data were also taken from the corresponding and appropriate initial region of the jet to ensure existence of a classical mixing layer. The initial jet spreading angle, or its growth rate, was then measured for all acquired images, and results along with those of others are presented in Figure 5. Of importance in this figure is the justification for the selection of the data sets and the nature of their measurements by other researchers. They are elaborated at sufficient detail in earlier papers. In order to gain a deeper appreciation of these selections, the reader is referred to Chehroudi et al. [10]. Therefore, they are only mentioned here in brief.

Because the jets investigated by Chehroudi et al. [5] exhibited both liquid-spray-like and gas-jet-like (two-phase and single-phase, resp.) appearances, depending on pressure (see Figure 1), appropriate comparisons with both liquid sprays (injected into a gas) and gas jets (injected into a gas) were justified and hence these results are presented in Figure 5. The simplest is the prediction of the linear growth or constant spreading angle for the turbulent incompressible submerged jet using the mixing length concept. Following Abramovich [14], a semiempirical equation was used which attempts to incorporate the effects of density variations by an introduction of a characteristic velocity (see Chehroudi et al. [10] for more details).

Brown and Roshko [15] measured spreading angles for a subsonic, two-dimensional, incompressible, turbulent mixing layer in which helium and nitrogen were used. Brown [16] (for a temporally growing mixing layer) and Papamoschou and Roshko [17] proposed a theoretical equation for incompressible variable-density gaseous mixing layers. Finally, Dimotakis [18] used the observation that, in general, the entrainment into the mixing layer from each stream was not the same and, in a system moving with a convection velocity, offered a geometrical argument to derive an equation for two-dimensional incompressible variable-density mixing layers. Chehroudi et al. [5] included predictions from these models as shown in Figure 5. Results by Richards and Pitts [19] for variable-density jets are also included.

Because both liquid-spray-like and gas-jet-like visual behaviors were observed, the growth rate for the liquid sprays produced from single-hole nozzles, typical of the ones used in diesel engines, was also incorporated in this figure. Figure 5 covers a density ratio of four orders of magnitude and is regarded as a unique and new plot in its own right. To some extent, and for comparable cases, disagreements between some results in this figure can be attributed to differences in the definition of the mixing layer thicknesses and the adopted measurement methods. For detailed discussion of this figure, see Chehroudi et al. [5, 10].

The important point which was stressed by Chehroudi et al. [10] is that for a range of density ratios in which images exhibit gas-jet-like appearance, the experimental data agrees well with the proposed theoretical equation by Dimotakis [18] and closely follows the trend of the Brown/Papamoschou and Roshko equation as shown in Figure 5. This can be taken as an important quantitative evidence that at supercritical pressures, the injected jets visually behave like a gas. Chehroudi's work appears to be the first time such a rigorous and quantitative evidence had been developed. The fractal dimension results discussed later provide additional evidence in support of this behavior.

Chehroudi et al. [20] also used the Raman scattering studies to measure density distributions. Initially, the growth rate measurements by them, using results acquired during the Raman scattering work, did not provide the same jet thickness values as those determined by the shadowgraphy approach. Apparently, as discussed by Brown and Roshko [15], different thickness definitions exist, and one can explore their relationship. Similar attempts in the context of supercritical jets showed that within the distances investigated, twice the full-width half-maximum (FWHM) of the Raman intensity radial profiles was equivalent to the thickness values measured through shadowgraphy. Realization of this relationship was very critical to consolidate the results from two different methodologies (Raman versus shadowgraphy). Figure 6 shows the growth rate measured using the Raman data in contrast to those determined through shadowgraph images.

These results were subsequently confirmed and extended by Oschwald and Micci [21] through a similar measurement technique. For example, they showed that when twice the FWHM of the Raman radial intensity profiles is used for

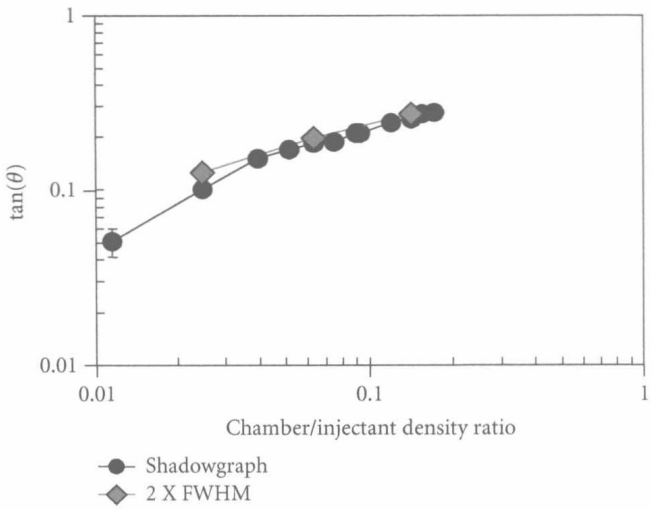

FIGURE 6: Comparison of the tangent of the spreading angle for a single jet of LN_2 injected into GN_2 measured using shadowgraph and Raman's techniques at twice the FWHM values. Chehroudi et al. [20].

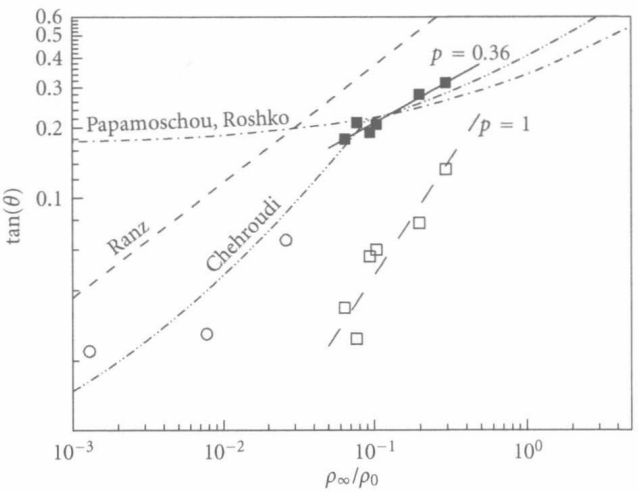

FIGURE 7: Comparison of the tangent of the spreading angle by Raman's techniques using twice the FWHM values (DLR data). Solid squares are for data from x/D of 15 to 32 whereas hollow squares are from x/D of 0.5 to 14. Chehroudi's model is also shown as dash-dot-dot curve. Single jet LN_2 into GN_2 with injector L/D = 11.6. Data from Oschwald and Micci [21]. Open circles are data points from Reitz and Bracco [7].

x/D values within 15 and 32, a good agreement exists between their results and those by Chehroudi's group (see the case designated as "p = 0.36" in Figure 7, where "p" is the exponent of the curve fitted through the data). However, the twice FWHM criterion did not fully agree with shadowgraphs for $x/D < 15$ in the study conducted by Oschwald and Micci [21] (see the case identified as "p = 1.0" in Figure 7).

Note that Oschwald and Micci [21] measured a larger range of axial distances and found that the criterion was not universal at extended ranges. There are several reasons why different trends might be observed at different distances.

It has to do with the fact that shadowgraphy and Raman scattering approaches measure different physical properties. The Raman signal is taken to be proportional to density whereas shadowgraphy is sensitive to the gradients of the density distribution. Thus a unique relationship between the results measured by the two methods may only be valid for a limited region and/or perhaps specific configurations. Recall that the data discussed above were obtained from injectors with different L/D ratios. Another potential cause, and hence discrepancies, is errors in attempting to perform Raman's measurements close to the injector inlet where density variations and thus index of refraction variations can be very large.

2.4. Fractal Dimension of the Interface. Fractals are intimately connected to the concept of self-similarity; see Mandelbrot [22]. The fractal dimension of any curve is between 1 and 2. The more wrinkled and space-filling a curve is, the larger the values of its fractal dimension. Natural curves, such as the outline of a cauliflower, are self-similar only to that within a narrow range of scales. The objective of the analysis here was to measure the fractal dimension of the interface of jets injected into the chamber in order to see if any pattern was uncovered.

The fractal dimension of jets at various pressures ranging from subcritical to supercritical was calculated and compared to results by other researchers. Reference results were taken from Sreenivasan and Meneveau [23] who measured the fractal dimensions of a variety of turbulent gaseous jets, mixing layers, and boundary layers. These results indicated a fractal dimension between 1.33 and 1.38. In addition, the fractal dimensions of a turbulent water jet (Dimotakis et al. [18]) and of a liquid jet in the second wind-induced atomization regime (Taylor and Hoyt [24]) were computed from high-resolution scanned images.

The fractal dimensions from the above reference cases are shown as horizontal lines in Figure 8. Overlaid on top of these lines are discrete points indicating the fractal dimension of LN_2 jets injected into GN_2 at various chamber pressures. One sees that at supercritical chamber pressures, the fractal dimension approaches a value similar to gaseous turbulent jets and mixing layers. As the chamber pressure is decreased, the fractal dimension also decreases. Below a reduced pressure of 0.8, the fractal dimension rapidly declines to a value approximately equal to that of liquid sprays in the second wind-induced liquid jet break-up regime.

A detailed discussion of the above results is also found in Chehroudi et al. [25, 26]. The key conclusion reached by Chehroudi's group is that the results from fractal analysis complement and extend the imaging data they acquired for the initial jet growth rate. At supercritical pressures, jets have a fractal dimension similar to turbulent gas jets, and at subcritical pressures, cryogenic jets have a fractal dimension similar to liquid sprays. The transition occurs at about the same chamber pressure as that when the transition in visual appearance and growth rate data discussed in Figure 5 takes place. Such distinctly different behaviors for jets under sub- and supercritical conditions were first demonstrated by

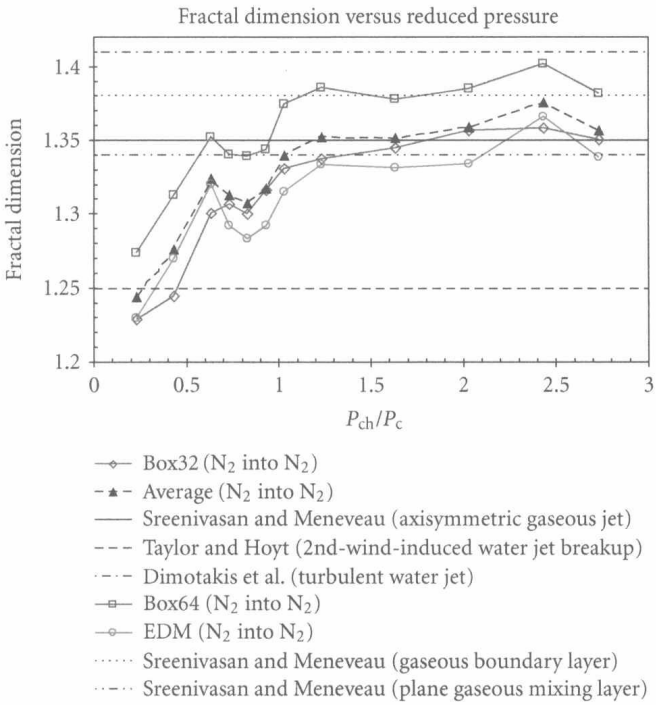

FIGURE 8: Fractal dimensions of the boundaries of various single jets as a function of reduced chamber pressure (chamber pressure divided by the critical pressure of the jet material). Discrete points are data from Chehroudi et al. [25, 26]. Box 32, Box 64, and EDM are different methods of calculating the fractal dimension, giving an impression of the extent of variability; for details, see Chehroudi et al. [25, 26].

Chehroudi's group in a quantitative manner using fractal analysis.

2.5. Measurement of the Dark-Core Length. Before presenting their results under supercritical conditions, Chehroudi et al. [25, 26] discussed some measurements from (gaseous and liquid) jets at subcritical conditions to set the stage and provide a contrast to their data. It is therefore useful to summarize what they recalled in their work.

According to Abramovich [14], the length of the "potential core" in isothermal uniform-density axisymmetric and two-dimensional jets is estimated to be about 6 to 10 injector diameters; whereas for nonisothermal cold jets injected into hot environments, it can reach up to about 25 injector diameters depending on jet temperature.

Also, according to Chehroudi et al. [27] the "intact core" length of the liquid sprays similar to the ones used in diesel engines is given by the equation $Cd_j(\rho_l/\rho_g)^{1/2}$ where ρ_l and ρ_g are liquid injectant and chamber gas densities, respectively, d_j is an effective jet exit diameter, and C is a constant between 3.3 and 11. This reflects an intact core length between 33 and 110 injector diameters for the chamber-to-injectant density ratio of 0.01 and between 16.5 and 55 diameters for the chamber-to-injectant density ratio of 0.04. These results are presented in Figures 9(a) and 9(b) for better comparison with what is measured for LN_2 injection into both sub- and supercritical GN_2 environment.

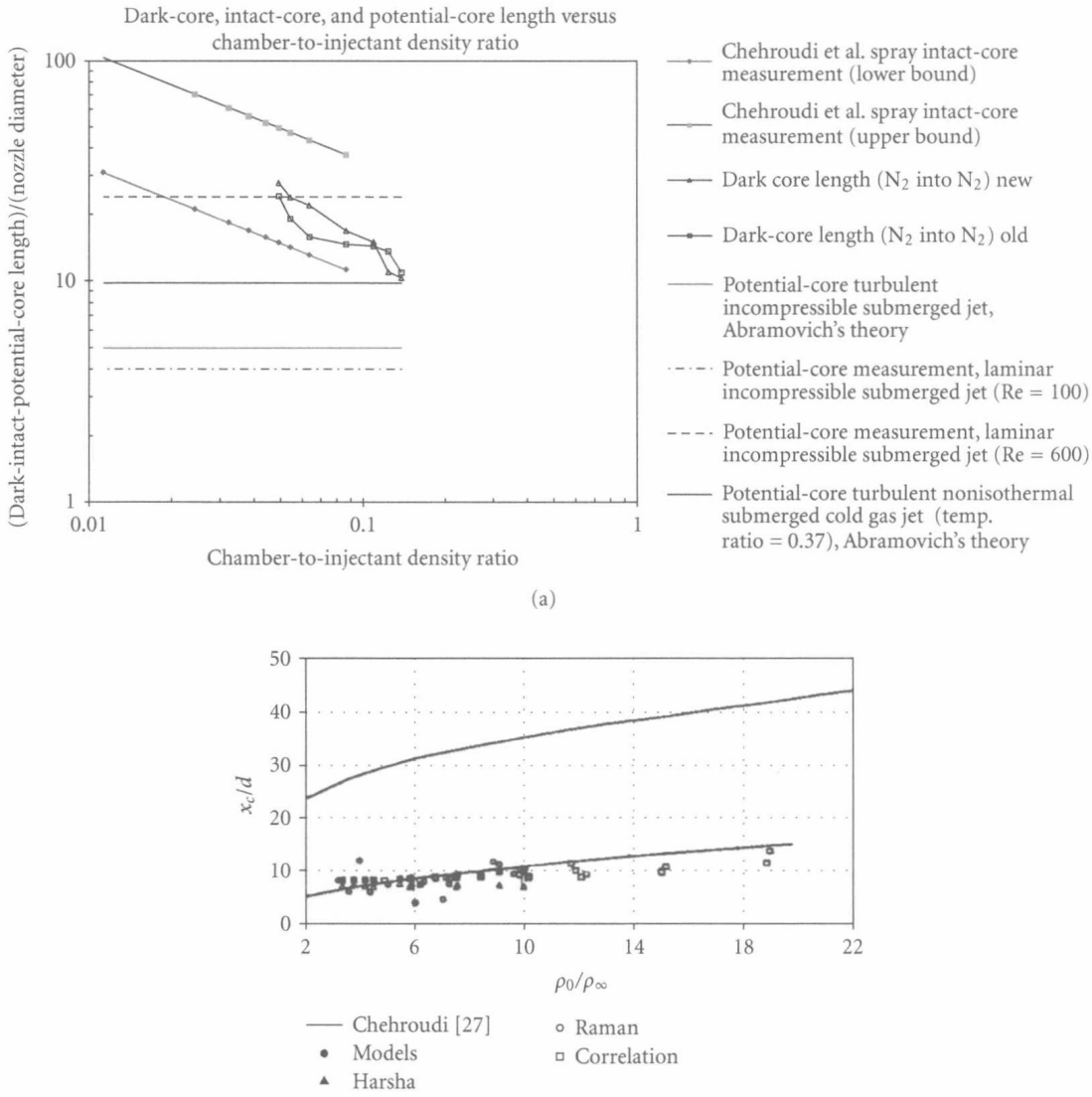

FIGURE 9: Ratio of either the dark-core, intact-core, or potential-core length, depending on the case, divided by the density ratio for single jets. (a): Chehroudi et al. [10], determined by analysis of shadowgraphs, for an injector $L/D = 200$. (b): Branam and Mayer [13], determined via Raman data, injector $L/D = 40$. Models: determined by computer simulation. Correlation: a correlation using a set of Raman's data by Branam and Mayer [13].

Considering that the classical two-stream mixing layer should start from the injector exit and extends to approximately the end of the potential core (or intact core) of the jet, Chehroudi et al. [5, 10] assumed that the jet "dark-core" region seen in their images played a similar role as the intact core or potential core. Figure 9(a) shows the dark-, intact-, or potential-core lengths normalized by the injector hole diameter plotted versus density ratio. By referring to Figure 9(a), Chehroudi et al. [5, 10] indicated that the growth rate data taken by them, which is presented earlier in Figure 1, was indeed from the corresponding and appropriate initial region to ensure existence of a classical mixing layer. They emphasized that it is only then when a valid comparison can be made (as they did) between their results and the two-stream mixing layers available in the literature. Finally, they found that the core length fluctuation levels at supercritical condition were several times lower than those observed at subcritical chamber pressures.

Complementary results by the Branam and Mayer [13] are also shown in Figure 9(b). These results were determined through a log-log plot of the centerline intensity measured by the Raman scattering to distinguish different flow regions. Note that the horizontal axis for Figures 9(a) and 9(b) are inverse of each other. The Branam and Mayer [13] data are at or below the lower bound of the Chehroudi et al. [27] model (i.e., solid curves in Figure 9(b)) which was proposed based on the liquid spray data in various atomization regimes. For chamber-to-injectant density ratios of less than 0.1 in Figure 9(a) (or injectant-to-chamber ratio of greater than 10 in Figure 9(b)), it appears that the Chehroudi et al. [25, 26]

experimental data shown in Figure 9(a) is larger by about a factor of 1.5 to 2 compared to the "correlation" given by Branam and Mayer [13] in Figure 9(b).

Considering that the raw data used by the two groups are from two different injectors and measurement methodologies, the agreement is considered adequate. However, further investigations are warranted.

2.6. Density and Temperature Fields. The main purpose of the Raman scattering measurements was to provide quantitative information and to enable mapping of the jet density field. Temperatures, for example, were calculated assuming application of a suitable equation of state. Radial density profiles were reported by Oschwald and Schik [28] in a normalized fashion. In this section, the centerline density and/or temperature profiles as functions of the axial distance from the injector exit plane and their self-similarity assessment are discussed.

The test conditions were chosen in order to assess the influence of the thermodynamic state of the injected cryogenic N_2 on the jet disintegration process. For example, above the critical pressure, the specific heat is finite but exhibits a maximum at a particular temperature. At this same point, the thermal diffusivity exhibits a minimum value. Three test cases were therefore investigated as shown in Figure 10(a). In test case A, the initial injection temperature is both above the critical temperature and above the temperature where the specific heat assumes a maximum value, whereas for test cases B and C the initial injection temperatures are both below the critical value and the temperature where the specific heat is at a maximum value.

Figures 10(b) and 10(c) show normalized centerline axial profiles of the density and temperature acquired by Oschwald and Schik [28] at a chamber pressure of 4 MPa (near the critical pressure of nitrogen). Note that the density decay behavior becomes slower as the initial injection temperature is decreased. The temperature profile, however, stays flat for up to a normalized distance (x/D) of about 25 to 30. They indicated that the development of the centerline temperature reflects the thermophysical properties of the nitrogen, being specific to the region where the specific heat reaches a maximum. For initial injection temperatures below the temperature where the specific heat reaches a maximum value, as the jet heats up, the fluid has to pass through a state with a maximum specific heat. The fluid temperature can then reach a value where a large amount of heat can be stored without any noticeable increase in temperature. It appears that the maximum specific heat line in a supercritical fluid results in a behavior similar to a liquid at its boiling point. That is, heat transfer to the nitrogen does not increase its temperature but simply expands the fluid (i.e., increases its specific volume). It is also for this reason that the dashed curves in Figure 10(a) are referred to as "pseudo boiling lines." Note that the density of the fluid varies strongly with temperature in this zone. At 6 MPa ($P_r = 1.76$, data not shown), the maximum of the specific heat is much less pronounced and the effects of the pseudo-boiling line is not as distinct as those seen under chamber pressure of 4 MPa. As shown by Oschwald and Schik [28], however, far downstream, it was observed that the temperature of the disintegrating and mixing supercritical fluid jet approached a value representative of a fully mixed jet but at a slower pace than that for the jet density.

The self-similarity of the density field has also been investigated by Chehroudi et al. [20] and the results are presented in Figure 11. According to Wygnanski and Fiedler [29], a fully self-preserved velocity field of a turbulent air jet should be observed at an x/D of greater than 40 when the Reynolds number is near 100,000. So et al. [30] reported self-preservation for x/D values larger than about 20 in a binary gas jet at Reynolds' number (Re) of about 4300. Although it appears that some inconsistencies exist for this criterion, one can see that for the near-critical and supercritical pressures, the density radial profiles approach the similarity model curve shown in Figure 11. The disagreement increases at subcritical pressures where the model is least applicable. It is worth indicating that results from a modeling and computational simulation by Zong et al. [31] also agrees well with Chehroudi's Raman scattering measurements.

Chehroudi et al. [20] using their Raman scattering data determined the FWHM of the radial density profiles at each axial distance from the injector, and the results, along with data by other investigators, are shown in Figure 12. More information on their experimental conditions is given in Table 1. Note that except for Chehroudi et al. [5, 25] and Oschwald et al. [32], all others performed injection of gaseous fluids into an ambient gas at subcritical pressures (based on the injectant critical pressure). Also, the FWHM was determined using the mass fraction profiles in both So et al. [30] and Richards and Pitts [19]. However, reported FWHM values by So et al. [30] using both density and mass fraction profiles were comparable. Chehroudi et al. [20] data in Figure 12 shows an increasingly larger spreading rate as chamber pressure is raised. The data at the supercritical condition ($P_r = 2.03$) approaches that of Richards and Pitts [19] acquired at a density ratio of 1.56 even though this ratio is substantially smaller than Chehroudi et al. [20] data. Results at larger distances were not available for their jet to enable a more comprehensive comparison between the cases.

Richards and Pitts [19] concluded that if care is exercised to ensure that the flow is free of buoyancy and coflow effects, the spreading rate in variable-density jets was independent of the initial density ratio, velocity profile, and turbulence level and conformed with the constant-density results of others. In addition, they proposed a slope in the range between 0.212 and 0.220 for the linear jet growth rate equation; see Figure 12. However, a linear least-square fit to Chehroudi et al. [20] data at $P_r = 2.03$ gives a slope of 0.102, almost half of that by Richards and Pitts [19]. One possible explanation for this difference is that Chehroudi's data covers a range much closer to the injector exit plane than that by Richards and Pitts [19], leading to a lowered growth rate value. A tendency towards higher growth rates can be seen if only the farthest two data points are considered in Chehroudi's data. However, a solid conclusion cannot be drawn based on these two points. It is also possible that at some high enough injectant-to-chamber density ratio, the spread rate universality indicated by Richards and Pitts breaks down and

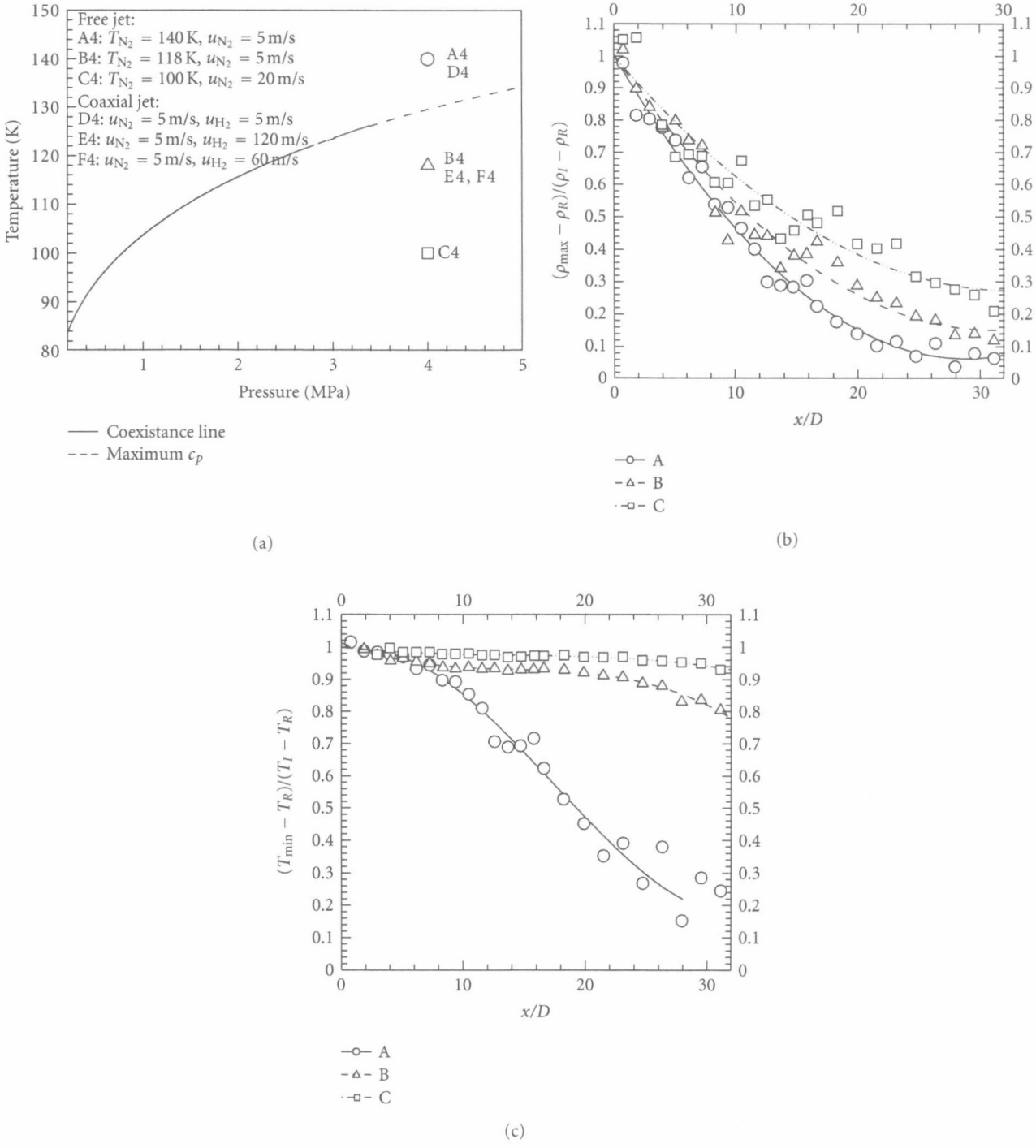

FIGURE 10: Normalized centerline density (b) and temperature (c) axial profiles of LN_2 injected into GN_2 at three different injection temperatures and a chamber pressure of 4 MPa (i.e., near critical pressure). The plot (a) shows the thermodynamic conditions under which test cases A, B, and C are conducted. The dashed line is the pseudoboiling line. Note, A4, B4, and C4 symbols represent A, B, and C cases, respectively. Oschwald and Schik [28].

one observes a somewhat retarded growth rate for variable-density turbulent jets. Some evidence in support of this position was given by Chehroudi et al. [20].

2.7. Phenomenological Model of the Jet Growth Rate. Using the experimental data collected on the growth of a cryogenic jet, a phenomenological model for the growth rate was proposed by Chehroudi et al. [5, 10] for the first time in the literature. Complete details on the development of this equation are to be found in these references. However, the physical reasoning motivating the proposed model equation is outlined below.

It was noticed by Chehroudi that previous expressions for the growth rate of liquid sprays and of turbulent jets have

TABLE 1: Some information extracted from works by other investigators reported here. T_{inj} and T_{ch} are injection and chamber temperatures. P_{ch} is chamber pressure. L/D is the injector hole-to-diameter ratio, x/D is the normalized distance from injector exit within which measurements were made. Chehroudi et al. [20].

	(Fluid inj./cham.)	T_{inj} K	P_{ch} MPa	T_{ch} K	Reduced pressure P_r	Inj./chamb. density ratio	Diameter D mm	L/D	x/D	Raynolds' number Re	Profile used to measure FWHM
Oschwald et al.	N_2/N_2	118	4	298	1.17	3.34	1.9	11.5	8.42	$1.2E+05$	Density
Oschwald et al.	N_2/N_2	140	4	298	1.17	12.5	1.9	11.5	1.05	$1.3E+05$	Density
Chehroudi et al.	N_2/N_2	95	6.9	295	2.03	7.1	0.505	100	4.8 to 24.4	$3.5E+04$	Density
Chehroudi et al.	N_2/N_2	110	1.5	295	0.43	40.6	0.505	100	4.8 to 24.5	$1.2E+04$	Density
So et al.	(He + Air)/Air	275	0.1	275	0.08	0.64	9.5		5.1	$5.0E+03$	Concentration and density
So et al.	(He + Air)/Air	275	0.1	275	0.08	0.64	9.5		6.4	$5.0E+03$	Concentration and density
Richards and Pitts	He into Air	275	0.1	275	0.44	0.138	6.35	~50	20–80	$4.0E+03$	Mass fraction
Richards and Pitts	C_3H_8 into Air	275	0.1	275	0.02	1.56	6.35	~50	40–120	$2.5E+04$	Mass fraction

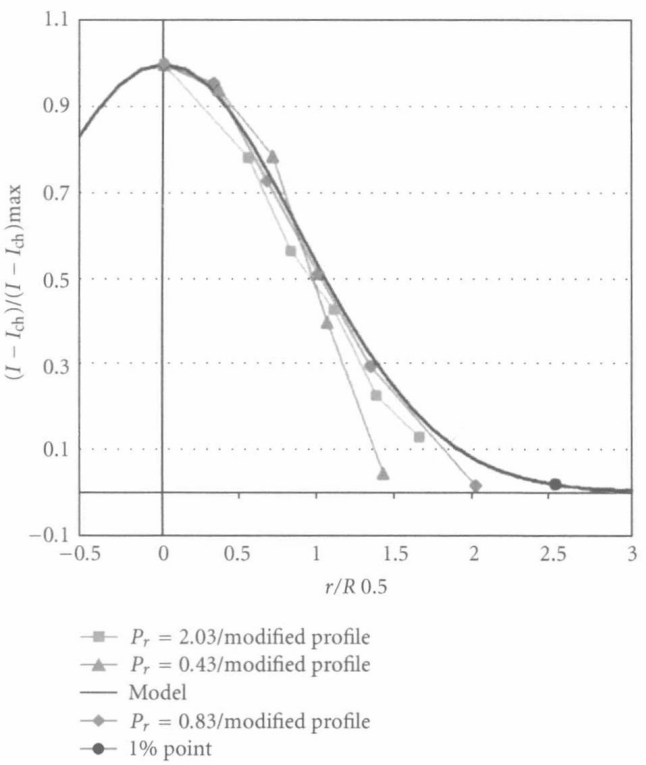

FIGURE 11: Plots of normalized intensity versus normalized radius for a single LN_2 jet injected into GN_2, at $x/D = 12.2$, at subcritical, near-critical, and supercritical pressures (Chehroudi et al. [20]). The solid curve is the self-similar model that represents data from a gaseous jet injected into a gaseous environment. I and I_{ch} symbols are measured intensities in the jet and in the chamber far away from the jet, respectively. Chehroudi et al. [20].

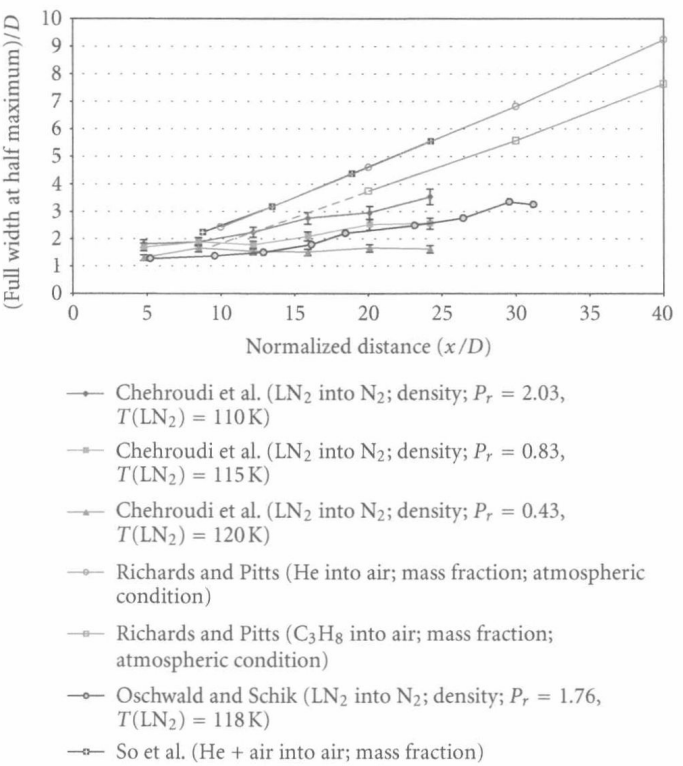

FIGURE 12: Normalized FWHM of the density-surplus radial profiles of single jets plotted as a function of the normalized axial distance from the injector exit plane. From Chehroudi et al. [20].

a remarkably similar form. For example, Reitz and Bracco [7] proposed that the growth rate of isothermal steady liquid sprays could be expressed as

$$\theta \approx 0.27\left[0 + \left(\frac{\rho_g}{\rho_l}\right)^{0.5}\right]. \quad (1)$$

The first term in the bracket is the number zero. This zero term was purposely kept to enable a comparison with other equations Chehroudi et al. [5, 10] discussed. They also referred to an equation proposed by Papamoschou and Roshko [17] for incompressible, but variable-density, turbulent gaseous jets:

$$\theta \approx 0.212\left[1 + \left(\frac{\rho_g}{\rho_l}\right)^{0.5}\right]. \quad (2)$$